Preprint typeset using LaTeX style emulateapj

A SUPERNOVA REGULATED ISM: SIMULATIONS OF THE TURBULENT MULTIPHASE MEDIUM

M. J. Korpi[1], A. Brandenburg[2], A. Shukurov[2], I. Tuominen[1], Å. Nordlund[3]

Draft version February 18, 1999

ABSTRACT

The dynamic state of the interstellar medium heated and stirred by supernovae (SNe) is simulated using a three-dimensional non-ideal MHD model in a domain extended 0.5×0.5 kpc horizontally and 2 kpc vertically, with gravitational field symmetric about the midplane of the domain, $z = 0$. We include both Type I and II SNe, allowing the latter to cluster in regions with enhanced gas density. The system segregates into two main phases, a warm denser phase and a hot dilute gas in global pressure equilibrium; there is also dense, cool gas compressed into filaments, shells and clumps by expanding SN remnants. The filling factor of the hot phase grows with height, so it dominates at $|z| \gtrsim 0.5$ kpc. The multi-component structure persists throughout the simulation and its statistical parameters show little time variation. The warm gas is in hydrostatic equilibrium supported by thermal and turbulent pressures. The multi-phase gas is in a state of developed turbulence. The r.m.s. random velocity is different in the warm and hot phases, $10\,\mathrm{km\,s^{-1}}$ and $40\,\mathrm{km\,s^{-1}}$, respectively, at $|z| \lesssim 1$ kpc; the turbulent cell size (twice the velocity correlation scale) is about 60 pc in the warm phase.

Subject headings: galaxies: ISM — ISM: kinematics and dynamics — turbulence — MHD

1. INTRODUCTION

The multi-phase structure of the interstellar medium (ISM) contributes to almost all aspects of its global dynamics, including its evolution, effects on magnetic fields and cosmic rays, and star formation. In a widely accepted picture (e.g., Heiles & Kulkarni 1987; Kulkarni & Heiles 1988; Spitzer 1990; McKee 1995), most of the volume is occupied by the hot ($T \simeq 10^6$ K), warm ($T \simeq 10^4$ K) and cold ($T \simeq 10^2$ K) phases, although molecular clouds and some transient phases can also be important in many respects. The main source of energy maintaining this complex structure are supernova (SN) explosions and stellar winds. The energy ejected by the SNe not only supports the hot phase, but also drives ubiquitous turbulence in all diffuse phases. Thus, turbulence and multi-phase structure are intrinsically connected features of the ISM, and in this paper we present a model describing them in a self-consistent manner.

2. THE MODEL

We model the ISM in the solar neighborhood using a local three-dimensional, non-ideal MHD model, which includes the effects of density stratification in the Galactic gravity field, heating via supernova explosions, radiative cooling, large scale shear due to Galactic differential rotation, compressibility, and magnetic fields, together with thermal conductivity and kinetic and magnetic viscosities. We adopt a local Cartesian frame of reference which rotates at an angular velocity $\Omega_0 = 25\,\mathrm{km\,s^{-1}\,kpc^{-1}}$ and assume a flat rotation curve. We solve for deviations $\boldsymbol{u}$ from this basic flow (Brandenburg et al. 1995). We solve the standard non-ideal MHD equations, namely the induction equation written for the magnetic vector potential, the momentum equation, the energy equation and the continuity equation. The vertical distribution of the gravitational acceleration is taken from Kuijken & Gilmore (1989) and includes contributions from a stellar disk and a spherical halo.

SN heating and radiative cooling are modelled by source and loss terms in the energy equation. SNe are introduced as instantaneous, localized explosive events releasing thermal energy $E_{\rm SN} = 10^{51}$ erg per SN. In practice, each explosion occurs during one computational time step, adjusted to be 10–100 years at the moment of explosion. To avoid the early, violent part of the free expansion phase, the injected energy has a Gaussian distribution with a width of 20 pc around the explosion site. This initial state of an individual SN remnant in our simulations corresponds to the beginning of the adiabatic stage of the expansion of a real remnant. The cooling function is adopted from Dalgarno & McCray (1972) and Raymond, Cox, & Smith (1976). With this cooling function, the gas at $T < 10^5$ K is thermally stable, so we deliberately suppress thermal instability at low temperatures and any dense phases possibly associated with it.

We include both Type I and II SNe in our calculations. For Type II SNe we take the SN rate per unit area $3 \times 10^{-5}\,\mathrm{yr^{-1}\,kpc^{-2}}$ corresponding to a frequency $1/44\,\mathrm{yr^{-1}}$ in the whole Galaxy and for Type I, $4 \times 10^{-6}\,\mathrm{yr^{-1}\,kpc^{-2}}$ corresponding to $1/330\,\mathrm{yr^{-1}}$ (Tammann, Löffler, & Schröder 1994). In the vertical direction we assume an exponential distribution of the SN explosion rate per unit volume. The SN scale heights adopted are 325 pc (Heiles 1987) and 90 pc (Miller & Scalo 1979) for Type I and II SNe, respectively. We choose the explosion site randomly in the horizontal plane, but exclude those positions where the density is less than the average in that layer; this prescription leads to a realistic fraction of clustered SNe.

[1]Department of Physical Sciences, Astronomy Division, University of Oulu, P. O. Box 333, 90571 Oulu, Finland

[2]Department of Mathematics, University of Newcastle, Newcastle upon Tyne NE1 7RU, UK

[3]Theoretical Astrophysics Center and Copenhagen University Observatory, Juliane Maries Vej, DK-2100 Copenhagen Ø, Denmark

For the initial state of the ISM we take a single thermal phase near hydrostatic equilibrium at a number density $0.6\,\mathrm{cm}^{-3}$, exponential scale height 100 pc and temperature 10^4 K, with a uniform, azimuthally directed, weak magnetic field of $0.1\,\mu$G strength, which will be rapidly amplified up to μG strength.

A detailed description of the code used is given by Brandenburg et al. (1995) and Nordlund & Stein (1990). The size of the computational domain is $0.5 \times 0.5 \times 2$ kpc in the radial, azimuthal and vertical directions, respectively. The Galactic symmetry plane, $z = 0$, is placed in the middle of the computational domain. The corresponding mesh size is $63 \times 63 \times 254$. The time step is 600 yr on average, but can be as short as 10–100 yr when SNe explode in a low density region resulting in very high expansion velocities. We adopt a shearing box approximation (Wisdom & Tremaine 1988) and apply periodic boundary conditions in azimuth, sliding periodic boundary conditions in radius, and open boundary conditions on the upper and lower faces of the computational domain. Matter is allowed to escape through the open boundaries, but any inflow is prohibited. This results in mass and energy loss through the top and bottom boundaries; in 100 Myr, about 10% of the total mass and energy escape from the computational domain. This makes our model applicable over only over a finite time interval.

Unlike earlier two-dimensional large-scale simulations of turbulent ISM (Rosen & Bregman 1995; Vázquez-Semadeni, Passot, & Pouquet 1995; Passot, Vázquez-Semadeni, & Pouquet 1995; Rosen, Bregman, & Kelson 1996; Scalo et al. 1998), our model is fully three-dimensional, so it captures more completely the evolution of vorticity and the development of interstellar turbulence and also admits realistic modelling of the turbulent dynamo action. However, we do not include star formation and self-gravity. We also neglect stellar winds because their contribution to interstellar turbulence is much less important than that of SNe (Abbott 1982; see also Rosen & Bregman 1995).

3. RESULTS AND DISCUSSION

3.1. *The Multi-Phase Structure*

Figure 1 shows snapshots of the density and velocity at different times. Only rarely can SN remnants remain spherically symmetric for times longer than 1 Myr because the ambient density distribution quickly becomes very nonuniform. Since the location of Type II SN explosions depends on the local density, 70% of Type II SNe are clustered producing large shells. The first shells appear at 10 Myr.

One can see a Type I SN remnant indicated by I at 20 Myr, shell structures produced by clustered Type II remnants, marked CII at 20, 40 and 60 Myr, and a narrow vertical channel (chimney) at 20 Myr between the two shells labeled CII. Another chimney can be seen at 60 Myr above and below the region marked CII. The shell structures are blown out by 5–10 SNe. Their diameter is 200–250 pc in the horizontal direction and 350–400 pc vertically, their lifetime is 10–15 Myr. The shell near the right-hand side of the 20 Myr frame breaks through the disk at 30 Myr via a narrow vertical channel. Other visually discernible structures in the snapshots are dense, cold filaments, shells and clumps produced by compression with resulting enhanced cooling. The densest structures in Fig. 1 have $n \simeq 20\,\mathrm{cm}^{-3}$ and temperatures of a few hundred degrees. The simulated shells and filaments are quite similar to those observed in H I (Verschuur 1974; Heiles 1979; Colomb, Pöppel, & Heiles 1980).

The system rapidly segregates into two phases, as can be seen from Fig. 2, where we present probability distribution functions (PDFs) of density, temperature and pressure logarithms averaged over six snapshots taken at intervals of 10 Myr at times 20–70 Myr. Two gas phases can be distinguished in the temperature PDF that has a well-pronounced double-maximum shape near the midplane where there are more or less equal amounts of the warm and hot gas. Based on this, we identify the gas at $T < 10^5$ K as the warm phase and that at higher temperatures, as the hot phase. Average gas density and temperature are $n_\mathrm{w} \simeq 0.1\,\mathrm{cm}^{-3}$, $T_\mathrm{w} \simeq 10^4$ K for the warm phase, and $n_\mathrm{h} \simeq 10^{-3}\,\mathrm{cm}^{-3}$, $T_\mathrm{h} \simeq 10^6$ K for the hot gas. Most of the warm gas is concentrated at $|z| \lesssim 500$ pc, whereas the hot gas is mainly located at larger heights. Therefore, the double-peaked structure of the temperature PDF gradually vanishes as height increases.

The PDF of the total pressure shown in Fig. 2c has a well pronounced peak at about $10^3\,\mathrm{K\,cm}^{-3}$, the value common for all the phases which does not change significantly with time (but varies with height — see Figs. 2c and 2f). The simulated ISM has clearly settled into statistical pressure equilibrium. At the evolutionary stage discussed, the total pressure is dominated by thermal and turbulent components with magnetic pressure still being 10^3 times smaller.

Since pressure distribution is rather broad, the warm and hot phases are not well separated in the density PDF where the double-peaked structure is pronounced only slightly. However, the appearance of Fig. 1 strongly suggests the presence of both the warm and the hot phases at all stages of evolution. At some times (e.g., 20 and 30 Myr), the density PDF also has two peaks, but the peaks are smeared by time averaging.

A typical maximum temperature within young SN remnants, as modelled here, is about 10^8 K. The temperature of the hot gas is about 10^6 K if only the temperature within an SN remnant at the moment of energy injection is above 10^7 K, which corresponds to the beginning of the adiabatic stage of the remnant evolution. The radiative cooling time exceeds 10^9 yr at $T = 10^6$ K, so the gas cools down mainly because of adiabatic expansion.

The position of the minimum in the temperature PDF that defines the distinction between the hot and warm phases is controlled by the temperature (10^5 K) at which the cooling function has a maximum. The density and temperature of the warm phase are controlled by the cooling rate: stronger cooling would result in denser and cooler gas (cf. Vázquez-Semadeni et al. 1996). Motivated by the form of the density and temperature PDFs, we define the borderline between the warm and cold components as $n \simeq 1\,\mathrm{cm}^{-3}$, $T \simeq 10^3$ K. It is not clear whether the dense, cold gas can be described as a separate physical phase in our simulations because it arises due to compression and is not supported by additional physical effects like self-gravity or thermal instability. Another important factor determining the density structures seen in the simulation

is the SN frequency and distribution: larger and denser structures develop if SNe are stronger correlated in space.

Type I SNe play an unexpected role in the overall dynamics. Since they can occur above the warm layer and push some gas downwards, they help gravity to prevent Type II SNe from ejecting warm gas to large heights as it occurred in the simulations of Rosen & Bregman (1995) and also in our other simulations without Type I SNe.

3.2. *Filling Factors and Density Profiles*

The volume filling factor of the hot gas ($T > 10^6$ K) over the whole domain is on the average 30–40% after the SNe have stirred the whole volume (this occurs approximately at 15 Myr). The filling factor of the hot gas grows with height from about 20–30% at the midplane to about 50–60% at $|z| = 300$ pc and 80–100% near $|z| = 1$ kpc. The filling factor is sensitive to the degree of SN correlation in space. We have also made runs with significantly lower degree of supernova correlation. Then the filling factor of the hot gas at $z = 0$ is $\simeq 60\%$ if SNe are completely randomly distributed as in the model of McKee & Ostriker (1977).

The time-averaged scale height of the warm gas is 180–200 pc, which is close to that under hydrostatic equilibrium supported by thermal and turbulent pressures. The density of the cold gas ($T < 10^3$ K) has a rather uneven vertical distribution, but it is mainly confined within $|z| \lesssim 100$ pc. Even though the hot phase is certainly far from hydrostatic equilibrium, its horizontally averaged density decreases smoothly with height at a scale of 600–700 pc.

3.3. *Interstellar Turbulence*

The velocity field in our simulations resembles fully developed turbulence. Many vortical structures (of a size $\simeq 100$ pc) can be seen in Fig. 1. The system is fed by thermal energy, and its partial conversion into kinetic energy occurs at late stages of the evolution of SN remnants when they reach pressure balance with the surrounding medium. For Type II SNe, this occurs when their radius is 50–100 pc, and for Type I SNe, which more often occur in low-density regions at large height, this radius is 100–150 pc (cf. McKee & Ostriker 1977). About 9% of the total energy of the SNe is converted into kinetic energy of the ISM. This is in a remarkable agreement with other estimates (e.g., Chevalier 1977; Thornton et al. 1998).

Statistical parameters of the velocity field are significantly different in different phases of the ISM. We show in Fig. 3 the autocorrelation function of the vertical velocity calculated in horizontal cross-sections at different heights for the warm and hot components separately. The correlation scale in the warm phase is $l_{\rm w} \simeq 30$ pc independently of z; this indicates a well-mixed turbulent layer with turbulent cells of $\simeq 60$ pc in size.

The correlation scale of the hot gas increases from $l_{\rm h} \simeq 20$ pc at the midplane (this is rather a typical radius of a chimney) to 60 pc at $z = 150$ pc. This correlation scale hardly characterizes turbulence in the hot phase, but rather reflects a typical size of a region occupied by the hot gas. A significant velocity correlation at large scales in the hot gas (see Fig. 3b) arises from systematic vertical outflow, a signature of the base of a galactic fountain.

The r.m.s. total velocity (obtained upon subtraction of any systematic component) remains fairly constant with z at about $v_{\rm w} \simeq 10\,{\rm km\,s^{-1}}$ and $v_{\rm h} \simeq 40\,{\rm km\,s^{-1}}$ for the warm and hot phases, respectively. These values agree remarkably well with observational estimates of turbulent velocities at small heights and in the Reynolds layer (Kulkarni & Fich 1985; Reynolds 1985; Wang, Heckman, & Lehnert 1997). For the cold gas, $v_{\rm c} \simeq 3\,{\rm km\,s^{-1}}$. The values of $v_{\rm w}$ and $v_{\rm c}$ are close to the speed of sound at the corresponding temperatures 2×10^4 and 10^3 K, whereas $v_{\rm h}$ is significantly smaller than $100\,{\rm km\,s^{-1}}$, the speed of sound at 10^6 K. However, the hot gas is involved in systematic vertical motion as it streams to the halo at a speed of 100–$200\,{\rm km\,s^{-1}}$. This kinetic energy can be transformed into disordered, turbulent motions, resulting in higher turbulent velocities in the halo. Random motions observed in the halo were reported to have an r.m.s velocity of $60\,{\rm km\,s^{-1}}$ (Kalberla et al. 1998).

4. CONCLUSIONS

Our model yields realistic temperature and density for both hot and warm phases of the ISM, which depend reasonably weakly on the model parameters. The turbulence parameters are significantly different in different phases of the ISM. The correlation scale of the warm gas remains constant with height, $l_{\rm w} \simeq 30$ pc at $|z| \lesssim 350$ pc. However, the correlation length of the hot has grows with height, apparently due to the expansion of rising hot bubbles and chimneys.

The warm gas appears to be in hydrostatic equilibrium with a scale height of about 200 pc; the cold gas has a patchy vertical distribution, but concentrates at $|z| \lesssim 100$ pc. The hot phase has a systematic upward motion, so it is away from any equilibrium at $|z| \leq 1$ kpc.

The filling factor of the hot phase $f_{\rm h}$ is a sensitive function of the SN rate, but depends only weakly on the SN distribution in z. For the parameters adopted above, $f_{\rm h}$ ranges from 20–30% at the midplane to 50–60% at $z = 300$ pc.

This work was supported by the EC Human Capital and Mobility Networks project No. ER-BCHRXCT940483. MK, AB and AS acknowledge financial support from PPARC grants PPA/G/S/1997/00284 and GR/L30268. The work of ÅN was partially supported by the Danish Research Foundation, through its establishment of the Theoretical Astrophysics Center.

REFERENCES

Abbott, D. C. 1982, ApJ, 263, 723
Brandenburg, A., Nordlund, Å., Stein, R. F., & Torkelsson, U. 1995, ApJ, 446, 741
Chevalier, R. A. 1977, ARA&A, 15, 175
Colomb, F. R., Pöppel, W. G. L., & Heiles, C. 1980, A&AS, 40, 47
Dalgarno, A., & McCray, R. A. 1972, ARA&A, 10, 375
Heiles, C. 1979, ApJ, 229, 533
Heiles, C. 1987, ApJ, 315, 555

Heiles, C., & Kulkarni, S. R. 1987, in Physical Processes in Interstellar Clouds, ed. G. E. Morfill & M. Scholer (Dordrecht: D. Reidel), 13
Kalberla, P. M. W., Westphalen, G., Mebold, U., Hartmann, D., & Burton, W. B. 1998, A&A, 332, L61
Kuijken, K., & Gilmore, G. 1989, MNRAS, 329, 605
Kulkarni, S. R., & Fich, M. 1985, ApJ, 289, 792
Kulkarni, S. R., & Heiles, C. 1988, in Galactic and Extragalactic Radio Astronomy, ed. G. L. Verschuur & K.I. Kellerman (Berlin: Springer), 95
McKee, C. F. 1995, in ASP Conf. Ser. 80, The Physics of the Interstellar Medium and Intergalactic Medium, ed. A. Ferrara, C. F. McKee, C. Heiles & P. R. Shapiro (San Francisco: ASP), 292
McKee, C. F., & Ostriker, J. P. 1977, ApJ, 218, 148
Miller, G. E., & Scalo, J. M. 1979, ApJS, 41, 513
Nordlund, Å., & Stein, R. F. 1990, Comput. Phys. Comm., 59, 119
Ostriker, J. P., & McKee, C. F. 1988, Rev. Mod. Phys., 60, 1
Passot, T., Vázquez-Semadeni, E., & Pouquet, A. 1995, ApJ, 455, 536
Raymond, J. C., Cox, D. P., & Smith, B. W. 1976, ApJ, 204, 290
Reynolds, R. J. 1985, ApJ, 294, 256
Rosen, A., & Bregman, J. N. 1995, ApJ, 440, 634
Rosen, A., Bregman, J. N., & Kelson, D. D. 1996, ApJ, 470, 839
Scalo, J., Vázquez-Semadeni, E., Chappell, D., & Passot, T. 1998, ApJ, 504, 835
Spitzer, L. 1990, ARA&A, 28, 71
Tammann, G. A., Löffler, W., & Schröder, A. 1994, ApJ, 92, 487
Thornton, K., Gaudlitz, M., Janka, H.-Th, & Steinmetz, M. 1998, ApJ, 500, 95
Vázquez-Semadeni, E., Passot, T., & Pouquet, A. 1995, ApJ, 441, 702
Verschuur, G. L. 1974, ApJS, 27, 65
Wang, J., Heckman, T. M., & Lehnert, M. D. 1997, ApJ, 491, 114
Wisdom, J., & Tremaine, S. 1988, AJ, 95, 925

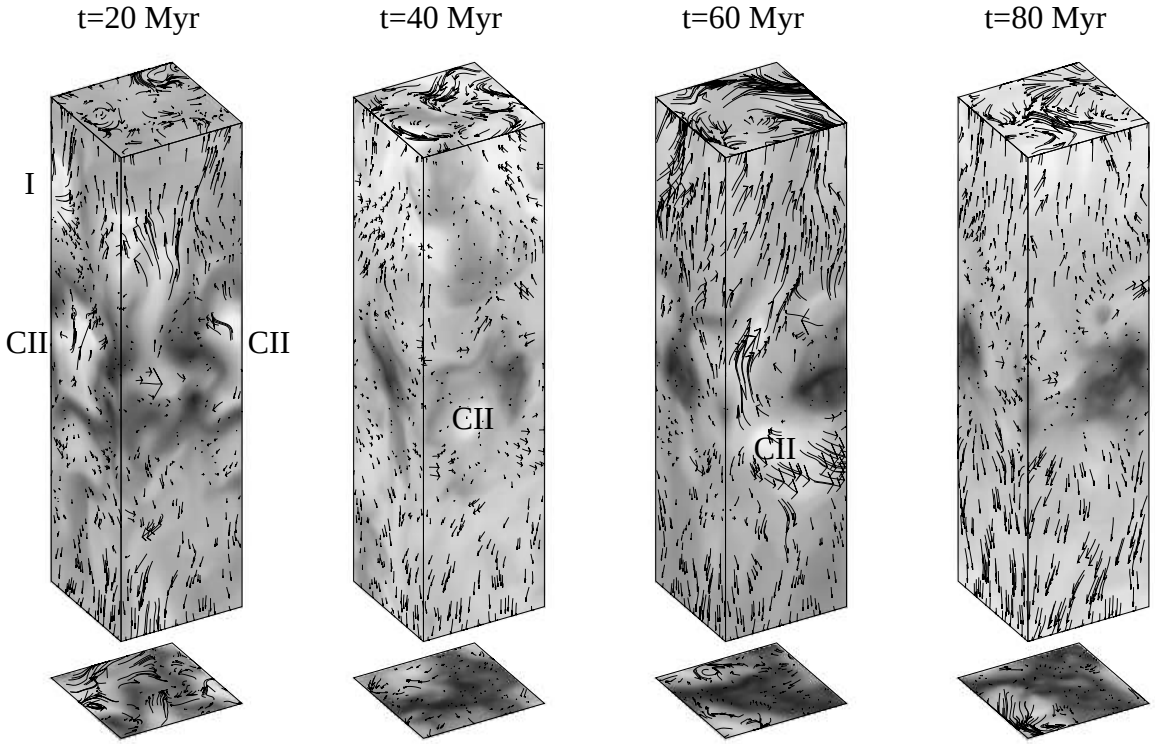

FIG. 1.— Gas density (shades of grey representing $\log n$) and velocity (vectors) on the faces of the computational domain (0.5×0.5 kpc horizontally and 2 kpc vertically) at different times in the simulation run. Frames below the boxes are mid-plane cross-sections. Darker regions correspond to larger densities. The density ranges in each snapshot are (from left to right) 8×10^{-6}–15 cm^{-3}, 1×10^{-4}–21 cm^{-3}, 5×10^{-6}–13 cm^{-3}, and 7×10^{-5}–17 cm^{-3}. On the vertical faces, vector length of 1 cm corresponds to 1000 km s^{-1}, and on the horizontal cross-sections 1 cm is 200 km s^{-1}.

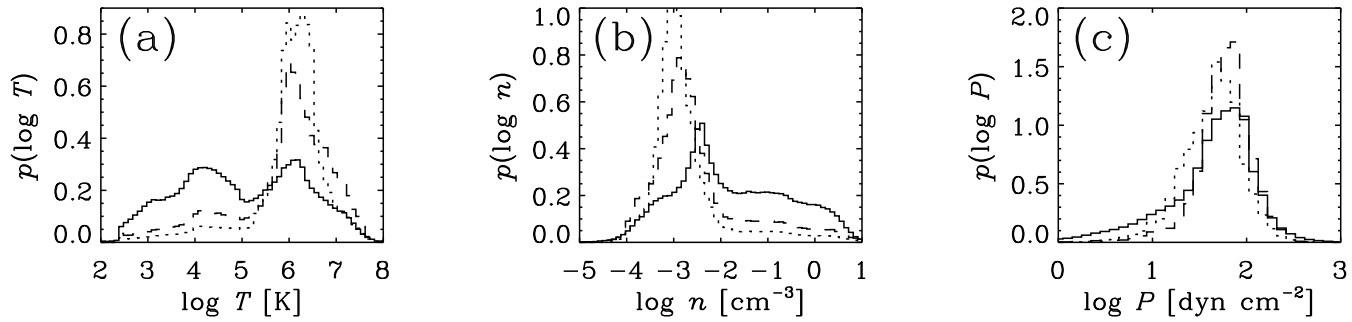

FIG. 2.— Probability density functions (PDFs) for logarithms of temperature (a), density (b), and total pressure (c) averaged over six snapshots taken at equal time intervals between 20 and 70 Myr and calculated for the whole computational volume for $|z| < 0.25$ kpc (solid), for $|z| < 0.5$ kpc (dashed) and $|z| < 1$ kpc (dotted).

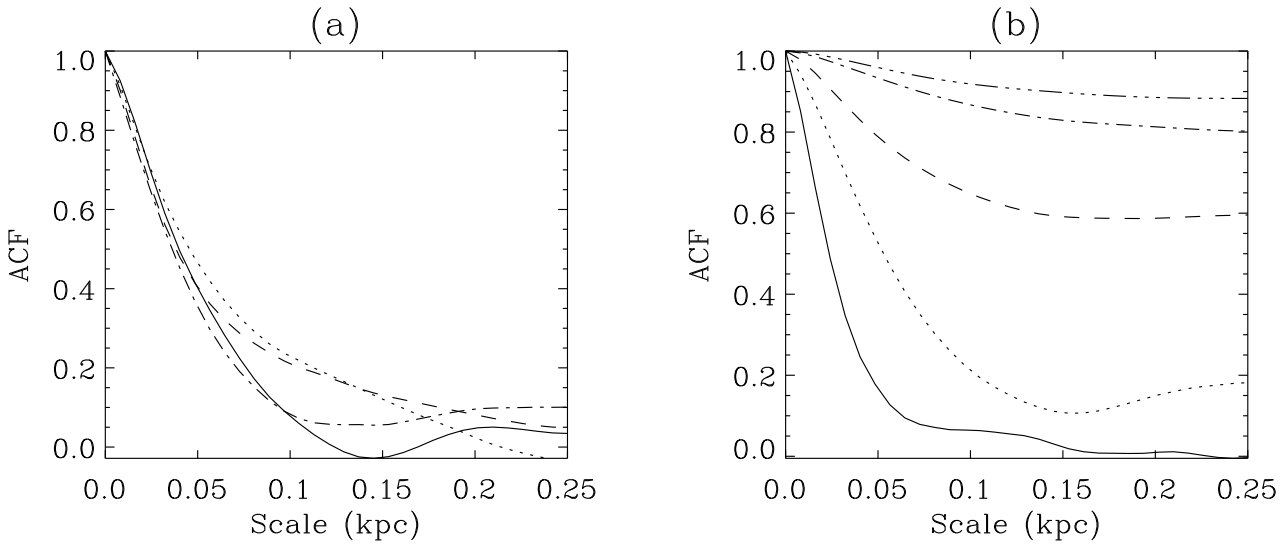

FIG. 3.— The autocorrelation function (ACF) of the vertical velocity for the warm and hot components separately at different heights obtained by averaging at times 60, 80 and 100 Myr. (a): warm gas at $z = 0$ (solid), 100 pc (dotted), 200 pc (dashed) and 300 pc (dashed-dotted). (b): hot gas at $z = 0$ (solid), 150 pc (dotted), 300 pc (dashed), 450 pc (dashed-dotted) and 850 pc (dashed-triple dotted).